Momentum distributions and spectroscopic factors of doubly-closed shell nuclei in correlated basis function theory

C. Bisconti[1,2,3], F. Arias de Saavedra[2] and G. Co'[1]

[1] *Dipartimento di Fisica, Università di Lecce and I.N.F.N., sezione di Lecce, I-73100 Lecce, Italy*

[2] *Departamento de Física Atómica, Molecular y Nuclear, Universidad de Granada, E-18071 Granada, Spain*

[3] *Dipartimento di Fisica, Università di Pisa, I-56100 Pisa, Italy*

(Dated: December 19, 2006)

Abstract

The momentum distributions, natural orbits, spectroscopic factors and quasi-hole wave functions of the ^{12}C ,^{16}O ,^{40}Ca ,^{48}Ca , and ^{208}Pb doubly closed shell nuclei, have been calculated in the framework of the Correlated Basis Function theory, by using the Fermi hypernetted chain resummation techniques. The calculations have been done by using the realistic Argonne v_8' nucleon-nucleon potential, together with the Urbana IX three-body interaction. Operator dependent correlations, which consider channels up to the tensor ones, have been used. We found noticeable effects produced by the correlations. For high momentum values, the momentum distributions show large enhancements with respect to the independent particle model results. Natural orbits occupation numbers are depleted by about the 10% with respect to the independent particle model values. Spectroscopic factors are in good agreement with the experimental values. The effects of the correlations are larger on the more deeply bound states.

PACS numbers: 21.60.-n; 21.10.Jx

I. INTRODUCTION

One of the major achievements of nuclear structure studies in the last ten years is the consolidation of the validity of the non relativistic many-body approach. The idea is to describe the nucleus with a Hamiltonian of the type:

$$H = -\frac{\hbar^2}{2m}\sum_{i}^{A}\nabla_i^2 + \sum_{i<j=1}^{A} v_{ij} + \sum_{i<j<k=1}^{A} v_{ijk} \ , \tag{1}$$

where the two- and three-body interactions, v_{ij} and v_{ijk} respectively, are fixed to reproduce the properties of the two- and three-body nuclear systems. The Schrödinger equation has been solved without approximations for few body systems [1] and light nuclei [2], up to A=12 [3]. The obtained results provide good descriptions, not only of the energies of these nuclei, but also of other observables.

The difficulties in extending to medium and heavy nuclei the techniques used in few body systems and light nuclei, favored the development of models, and of effective theories. The basic idea of the effective theories is to work in a restricted space of the many-body wave functions. Usually, one works with many-body wave functions which are Slater determinants of single particle wave functions. The idea of single particle wave functions implies the hypothesis of a mean-field where the various nucleons move independently one from the other. This Independent Particle Model (IPM) is quite far from the picture provided by the microscopic calculations quoted above, describing the nucleus as a many-body system of strongly interacting nucleons. In the Hartree-Fock theory, which provides the microscopic foundation of the IPM, the Hamiltonian is not any more that of Eq. (1), but it is an effective Hamiltonian built to take into account, obviously in an effective manner, the many-body effects that the microscopic calculations explicitly consider. The construction of effective interactions starting from the microscopic ones, covers a wide page of the nuclear physics history, starting from the Brueckner G-matrix effective interactions [4, 5], up to the recent V_{lowk} interaction [6, 7] and the interaction obtained by applying the unitary correlation operator method [8, 9].

The application of the IPM is quite successful, but there are evidences of the intrinsic limitations in its applicability. For example, the measured spectroscopic factors are systematically smaller than one [10–12], which is the value predicted by the IPM. The (e,e'p) cross sections in the quasi-elastic region need a consistent reduction of the IPM hole strength to

be explained [13, 14]. The same holds for the electromagnetic form factors of the low-lying states, especially those having large angular momentum [15, 16]. The emission of two like nucleons in photon and electron scattering process cannot be described by the IPM [17, 18]. Also the charge density distributions extracted by elastic electron scattering data are, in the nuclear interior, smaller than those predicted by the IPM [19, 20]. These examples indicate the presence of physics effects, commonly called correlations, which are not described by the IPM.

It is common practice to distinguish between long and short range correlations since they have different physical sources. The long-range correlations are related to collective excitations of the system, such as the giant resonances. The short-range correlations (SRC) are instead connected to the strongly repulsive core of the microscopic nucleon-nucleon interaction. The repulsive core reduces the possibility that two nucleons can approach each other, and this modifies the IPM picture where, by definition, the motion of each nucleon does not depend on the presence of the other ones.

Even though most of the calculations of medium heavy nuclei are based on the IPM, and on the effective theories, various techniques, aiming to attack the problem by using the microscopic Hamiltonian (1), have been developed. The Brueckner-Hartree-Fock approach has been recently applied to the ^{16}O nucleus [21]. No core-shell model calculations have been done for nuclei lighter than ^{12}C [22, 23]. The coupled cluster method has been used to evaluate ^{16}O properties [24, 25].

About fifteen years ago [26], we started a project aimed to apply to the description of medium and heavy nuclei the Correlated Basis Function (CBF) theory, successfully used to describe the nuclear and neutron matter properties [27, 28]. We solve the many-body Schrödinger equation by using the variational principle:

$$\delta E[\Psi] = \delta \frac{< \Psi | H | \Psi >}{< \Psi | \Psi >} = 0 \ . \tag{2}$$

The search for the minimum of the energy functional is done within a subspace of the full Hilbert space spanned by the A-body wave functions which can be expressed as:

$$\Psi(A) = \mathcal{F}(1, ..., A)\Phi(1, ..., A) \ , \tag{3}$$

where $\mathcal{F}(1, ..., A)$ is a many-body correlation operator and $\Phi(1, ..., A)$ is a Slater determinant composed by single particle wave functions, $\phi_\alpha(i)$. In our calculations, we used two-body

interactions of Argonne and Urbana type, and we considered all the interaction channels up to the spin-orbit ones. Together with these two-body interactions, we used the appropriated three-body forces of Urbana type. The complexity of the interaction required the use of operator dependent correlations. We consider correlations of the type:

$$\mathcal{F} = \mathcal{S}\left(\prod_{i<j=1}^{A} F_{ij}\right) \ , \tag{4}$$

where $\mathcal{S}$ is a symmetrizer operator and F_{ij} is expressed in terms of two-body correlation functions f_p as:

$$F_{ij} = \sum_{p=1}^{6} f_p(r_{ij}) O_{ij}^p \ . \tag{5}$$

In the above equation we have adopted the nomenclature commonly used in this field, by defining the operators as:

$$O_{ij}^{p=1,6} = [1, \boldsymbol{\sigma}_i \cdot \boldsymbol{\sigma}_j, S_{ij}] \otimes [1, \boldsymbol{\tau}_i \cdot \boldsymbol{\tau}_j] \ , \tag{6}$$

where $\boldsymbol{\sigma}_i$ and $\boldsymbol{\tau}_i$ indicate the usual Pauli spin and isospin operators, and $S_{ij} = (3\hat{\mathbf{r}}_{ij} \cdot \boldsymbol{\sigma}_i \hat{\mathbf{r}}_{ij} \cdot \boldsymbol{\sigma}_j - \boldsymbol{\sigma}_i \cdot \boldsymbol{\sigma}_j)$ is the tensor operator.

We recently succeeded in formulating the Fermi Hypernetted Chain (FHNC) equations, in Single Operator Chain (SOC) approximation, for nuclei non saturated in isospin, and with single particle basis described in a jj coupling scheme. We presented in Ref. [29] the binding energies and the charge distributions of ^{12}C , ^{16}O , ^{40}Ca , ^{48}Ca and ^{208}Pb doubly closed shell nuclei obtained by using the minimization procedure (2). These calculations have the same accuracy of the best variational calculations done in nuclear and neutron matter [27, 28].

In the present article, we show the results of our study, done in the FHNC/SOC computational scheme, on some ground state quantities related to observables. They are momentum distributions, natural orbits and their occupation numbers, quasi-hole wave functions and spectroscopic factors. We used the many-body wave functions obtained in Ref. [29] with the Argonne v_8' two-nucleon potential, together with the Urbana XI three-body force. We have calculated momentum distributions also with the wave functions produced by another interaction, the Urbana v_{14} truncated up to the spin-orbit terms, implemented with the Urbana VII three-body force. The results obtained with this last interaction do not show relevant differences with those obtained with the v_8' and UIX interaction, therefore we do not present them.

The paper is organized as follows. In Sect. II we present the results of the One-Body Density Matrix (OBDM) and of the momentum distribution. In Sect. III we discuss the natural orbits, i.e. the single particle wave functions forming the basis where the OBDM is diagonal. In Sect. IV we present our results about the quasi-hole wave functions and in Sect. V we summarize our results and draw our conclusions.

II. ONE-BODY DENSITY MATRIX AND MOMENTUM DISTRIBUTION

We define the one-body density matrix, (OBDM), of a system of A nucleons as:

$$\begin{aligned}\rho(x_1, x_1') &\equiv \sum_{s,s',t} \rho^{s,s';t}(\mathbf{r}_1, \mathbf{r}_1')\, \chi_s^\dagger(1)\chi_t^\dagger(1)\chi_{s'}(1')\chi_t(1') \\ &\equiv \frac{A}{<\Psi|\Psi>} \int dx_2 \ldots dx_A \Psi^\dagger(x_1, x_2, \ldots, x_A)\Psi(x_1', x_2, \ldots, x_A) \ . \end{aligned} \tag{7}$$

In the above expression, the variable x_i indicates the position ($\mathbf{r}_i$) and the third components of the spin (s_i) and of the isospin (t_i) of the single nucleon. The $\chi(i)$ functions represent the Pauli spinors. With the integral sign we understand that also the sum on spin and isospin third components of all the particles from 2 up to A, is done. In our calculations we are interested in the quantity:

$$\rho^t(\mathbf{r}_1, \mathbf{r}_1') = \sum_{s=\pm 1/2} \left[\rho^{s,s;t}(\mathbf{r}_1, \mathbf{r}_1') + \rho^{s,-s;t}(\mathbf{r}_1, \mathbf{r}_1')\right] \ , \tag{8}$$

whose diagonal part ($\mathbf{r}_1' = \mathbf{r}_1$) represents the one-body density of neutrons or protons, this last one related to the charge density distribution of the nucleus.

We obtain the momentum distributions of protons or neutrons as:

$$n^t(k) = \frac{1}{\mathcal{N}_t} \int d\mathbf{r}_1 d\mathbf{r}_1'\, e^{i\mathbf{k}\cdot(\mathbf{r}_1 - \mathbf{r}_1')} \rho^t(\mathbf{r}_1, \mathbf{r}_1') \ , \tag{9}$$

where we have indicated with $\mathcal{N}_t$ the number of protons or neutrons. The above definitions imply the following normalization of $n(k)$:

$$\int d\mathbf{k}\, n^t(k) = (2\pi)^3 \ . \tag{10}$$

We describe doubly closed shell nuclei, with different numbers of proton and neutrons, in a jj coupling scheme. The most efficient single particle basis to be used is constructed by a set of single particle wave functions expressed as:

$$\phi^t_{nljm}(\mathbf{r}_i) = R^t_{nlj}(r_i) \sum_{\mu,s} < l\mu \frac{1}{2} s|jm > Y_{l\mu}(\Omega_i)\chi_s(i)\chi_t(i) = R^t_{nlj}(r_i)\mathbf{Y}^m_{lj}(\Omega_i)\chi_t(i) \ . \tag{11}$$

In the above expression we have indicated with $Y_{l\mu}$ the spherical harmonics, with $<|>$ the Clebsch-Gordan coefficient, with $R^t_{nlj}(r_i)$ the radial part of the wave function, and with $\mathbf{Y}^m_{lj}$ the spin spherical harmonics [30].

The uncorrelated OBDMs, those of the IPM, are obtained by substituting in Eq. (7) the correlated function $|\Psi>$ with the Slater determinant $|\Phi>$ formed by the single particle wave functions (11). We obtain the following expressions:

$$\rho^t_o(\mathbf{r}_1,\mathbf{r}'_1) = \sum_s \left[\rho^{s,s;t}_o(\mathbf{r}_1,\mathbf{r}'_1) + \rho^{s,-s;t}_o(\mathbf{r}_1,\mathbf{r}'_1)\right] \ , \tag{12}$$

$$\rho^{s,s;t}_o(\mathbf{r}_1,\mathbf{r}'_1) \ = \ \frac{1}{8\pi}\sum_{nlj}(2j+1)R^t_{nlj}(r_1)R^t_{nlj}(r'_1)P_l(\cos\theta_{11'}) \ , \tag{13}$$

$$\rho^{s,-s;t}_o(\mathbf{r}_1,\mathbf{r}'_1) \ = \ \frac{1}{4\pi}\sum_{nlj}(-1)^{j-l-1/2}R^t_{nlj}(r_1)R^t_{nlj}(r'_1)\sin\theta_{11'}P'_l(\cos\theta_{11'}) \ . \tag{14}$$

In the above equations $\theta_{11'}$ indicates the angle between $\mathbf{r}_1$ and $\mathbf{r}'_1$, P_l and P'_l the Legendre polynomials and their first derivative respectively. The presence of the second term of Eq. (12), the antiparallel spin terms given in Eq. (14), is due the jj coupling scheme required to describe heavy nuclei.

The correlated OBDM is obtained by using the ansatz (3) in Eq. (7). This calculation is done by using the cluster expansion techniques as indicated in [31] and [32], where only scalar correlations have been used, and in [33], where the state dependent correlations have been used, but in a ls coupling scheme. We followed the lines of Ref. [33] but we consider, in addition, the presence of the antiparallel spin terms and we distinguish proton and neutron contributions. The explicit expression of the OBDM, in terms of FHNC/SOC quantities, such as two-body density distributions, vertex corrections, nodal diagrams etc., is given in Appendix A. The diagonal part of the OBDM is the one-body density, normalized to the number of nucleons. Because of this, the momentum distribution satisfies the following sum rules:

$$S^t_0 = \frac{1}{(2\pi)^3}\int d\mathbf{k}\, n^t(k) = 1 \ , \tag{15}$$

and

$$S^t_2 = \frac{1}{(2\pi)^3}\frac{\hbar^2}{2m}\int d\mathbf{k}\, k^2\, n^t(k)/T^t_{FHNC} = 1 \ , \tag{16}$$

where we have indicated with T^t_{FHNC} the kinetic energy of the protons ($t = 1/2$) or neutrons ($t = -1/2$).

We have verified the accuracy of our calculations by testing the exhaustion of the above sum rules for each $n(k)$. We found that the sum rules were always satisfied at the level of few parts on a thousand. In any case, we found that the sum rules are even better satisfied when only scalar correlations are used.

The surface shown in Fig.1 represents the proton OBDM of the ^{208}Pb nucleus, for $\theta_{11'}$=0. We have shown in [29] that the SRC lower the one-body proton distribution, and also that of the neutrons, in the nuclear center. In order to highlight the effects of the correlations on the density matrix, we show in Fig. 2 the quantity $\rho_o(r_1, r_1') - \rho(r_1, r_1')$. It is interesting to notice that the major differences between the OBDMs are not in the diagonal part, but just beside it. The consequences of these, small, differences between the OBDMs on the momentum distributions, are shown in Fig. 3. In this figure, we compare the ^{12}C , ^{16}O , ^{40}Ca , ^{48}Ca and ^{208}Pb momentum distributions calculated in the IPM model, with those obtained by using scalar and operator dependent correlations.

The general behavior of the momentum distributions, is very similar for all the nuclei we have considered. Correlated and IPM distributions almost coincide in the low momentum region up to a precise value, when they start to deviate. The correlated distributions show high momentum tails, which are orders of magnitude larger than the IPM results. The value of k where uncorrelated and correlated momentum distributions start to deviate, is smaller the heavier is the nucleus. It is about 1.9 fm^{-1} for ^{12}C , and 1.5 fm^{-1} for ^{208}Pb . We notice that the value of the Fermi momentum of symmetric nuclear matter at the saturation point is 1.36 fm^{-1}.

The results presented in Fig. 3 clearly show that the effects of the scalar correlations are smaller than those obtained by including the operator dependent terms. We shall see in the following that this is a common feature of our results.

Since relatively small differences are compressed in logarithmic scale, we use the linear scale in Fig. 4 to show, as examples, the proton momentum distributions for ^{16}O and ^{208}Pb nuclei, multiplied by k^2. This quantity, multiplied by a factor $(2\pi)^3$, is the probability of finding a proton with momentum k. We observe that the effects of the SRC on the quantity shown in Fig. 4 are basically two. The first one is the already mentioned enhancement at large values of k. This effect is less evident here than in Fig. 3. The second effect of the SRC is a reduction of the maxima which appear approximately at k=1 fm^{-1} in both nuclei, and it is hardly visible in Fig. 3. These two effects are obviously related, since all

the momentum distributions are normalized as indicated by Eq. (15), therefore reductions and increases must compensate.

In our calculations, we found that the proton and neutron momentum distributions for nuclei with $N = Z$ are very similar. For this reason we do not show the neutron momentum distributions of ^{12}C , ^{16}O and ^{40}Ca . On the other hand, we compare in Fig. 5 the proton and neutron momentum distributions of ^{48}Ca and ^{208}Pb . In both nuclei, the difference between these two distributions is mainly in the region where the IPM picture dominates. In an infinite fermions system, the larger is the density, the larger is the Fermi momentum. This property is present also in finite systems, even though the single particle wave functions are no longer eigenstates of the momentum. In the figure, this fact is clearly shown by the shift of the neutron IPM momentum distributions, with respect to that of the protons. When the distributions start to be dominated by the SRC effects, the protons and neutrons results are very close. This is an indication that shell and surface effects are irrelevant in the high momentum region and the SRC effects are in the average the same for protons and neutrons.

The increase of the momentum distribution at large k values, induced by the SRC is a well known result in the literature, see for example the review of Ref. [34]. The momentum distributions of medium-heavy nuclei, have been usually obtained by using approximated descriptions of the cluster expansion, which is instead considered at all orders in our treatment. The importance of a complete description of the cluster expansion is exemplified in Fig. 6, where, together with our results, we also show the results of Ref. [35], obtained by truncating the cluster expansion to the first order in the correlation lines. In both calculations the same correlation functions and single particle basis, those of Ref. [29], have been used. The results obtained with the first order approximation, provide only a qualitative description of the correlation effects. They show high-momentum enhancements which, however, underestimate the correct results by orders of magnitude.

III. NATURAL ORBITS

The natural orbits are defined as those single particle wave functions forming the basis where the OBDM is diagonal:

$$\rho^t(\mathbf{r}_1, \mathbf{r}'_1) = \sum_{nlj} c^t_{nlj} \phi^{*\,t,NO}_{nlj}(\mathbf{r}_1) \phi^{t,NO}_{nlj}(\mathbf{r}'_1) \ . \tag{17}$$

In the above equation the c^t_{nlj} coefficients, called occupation numbers, are real numbers. In the IPM, the natural orbits correspond to the mean-field wave functions of Eq. (11), and the c^t_{nlj} numbers are 1, for the states below the Fermi surface, and 0 for those above it.

In order to obtain the natural orbits, we found convenient to express the OBDM of Eq. (17) as:

$$\rho^t(\mathbf{r}_1,\mathbf{r}_{1'}) = A^t(\mathbf{r}_1,\mathbf{r}_{1'})\rho^t_o(\mathbf{r}_1,\mathbf{r}_{1'}) + B^t(\mathbf{r}_1,\mathbf{r}_{1'}) \ , \tag{18}$$

where $\rho^t_o(\mathbf{r}_1,\mathbf{r}_{1'})$ is the uncorrelated OBDM of Eq. (12), and the other two quantities are defined as:

$$\begin{aligned} A^t(\mathbf{r}_1,\mathbf{r}'_1) \ &= \ 2C^t_{\omega,SOC}(\mathbf{r}_1)C^t_{\omega,SOC}(\mathbf{r}'_1)\exp[N^t_{\omega\omega}(\mathbf{r}_1,\mathbf{r}'_1)] + \\ &\quad 2C^t_{\omega}(\mathbf{r}_1)C^t_{\omega}(\mathbf{r}'_1)\exp[N^t_{\omega\omega}(\mathbf{r}_1,\mathbf{r}'_1)]\sum_{p>1}A^k\Delta^k N^t_{\omega\omega,p}(\mathbf{r}_1,\mathbf{r}'_1) \ , \qquad (19) \\ B^t(\mathbf{r}_1,\mathbf{r}'_1) \ &= \ -2C^t_{\omega,SOC}(\mathbf{r}_1)C^t_{\omega,SOC}(\mathbf{r}'_1)\exp[N^t_{\omega\omega}(\mathbf{r}_1,\mathbf{r}'_1)]N^t_{\omega_c\omega_c}(\mathbf{r}_1,\mathbf{r}'_1) - \\ &\quad 2C^t_{\omega}(\mathbf{r}_1)C^t_{\omega}(\mathbf{r}'_1)\exp\left[N^t_{\omega\omega}(\mathbf{r}_1,\mathbf{r}'_1)\right] \\ &\quad \times\sum_{p>1}A^k\Delta^k\Big\{N^t_{\omega\omega,p}(\mathbf{r}_1,\mathbf{r}'_1)N^t_{\omega_c\omega_c}(\mathbf{r}_1,\mathbf{r}'_1) + N^t_{\omega_c\omega_c,p}(\mathbf{r}_1,\mathbf{r}'_1)\Big\} \ . \qquad (20) \end{aligned}$$

The meaning of the $\omega\omega$, $\omega_c\omega_c$ labels used in the above equations have been defined in [33] where the index k has been defined as $p = 2k + l - 1$ with $l = 0, 1$ and $p = 1, \ldots, 6$. The detailed expressions of the vertex corrections C and of the nodal functions N are given in Appendix A.

We expand the OBDM on a basis of spin spherical harmonics $\mathbf{Y}^m_{lj}$, Eq. (11),

$$\rho^t(\mathbf{r}_1,\mathbf{r}'_1) = \sum_{ljm}\frac{1}{2j+1}\left[\mathcal{A}^t_{lj}(r_1,r'_1) + \mathcal{B}^t_{lj}(r_1,r'_1)\right]\mathbf{Y}^{*m}_{lj}(\Omega_1)\mathbf{Y}^m_{lj}(\Omega'_1) \tag{21}$$

where Ω_1 and Ω'_1 indicate the polar angles identifying $\mathbf{r}_1$ and $\mathbf{r}'_1$. The explicit expressions of the $\mathcal{A}$ and $\mathcal{B}$ coefficients are:

$$\begin{aligned} \mathcal{A}^t_{lj}(r_1,r'_1) \ &= \ (2l+1)\sum_{n_2l_2j_2l}(2l_2+1)(2j_2+1)\begin{pmatrix} l & l_1 & l_2 \\ 0 & 0 & 0 \end{pmatrix}^2\begin{Bmatrix} j_2 & l_1 & j \\ l & 1/2 & l_2 \end{Bmatrix}^2 \\ &\quad R^t_{nl_2j_2}(r_1)R^t_{nl_2j_2}(r_2)A^t_{l_1}(r_1,r'_1) \qquad (22) \end{aligned}$$

with

$$A^t_l(r_1,r'_1) = \frac{2}{2l+1}\int d\Omega A^t(\mathbf{r}_1,\mathbf{r}'_1)P_l(\cos\theta_{11'}) \tag{23}$$

and

$$\mathcal{B}^t_{lj}(r_1,r'_1) = \frac{4\pi}{2l+1}\int d(\cos\theta_{11'})B^t(\mathbf{r}_1,\mathbf{r}'_1)P_l(\cos\theta_{11'}) \tag{24}$$

In the above equations we have used the 3j and 6j Wigner symbols [30]. The term $\mathcal{A}$ depends on both orbital and total angular momenta of the single particle, l and j respectively, and the term $\mathcal{B}$ depends only on the orbital angular momentum l.

As an example of our results, we show in Figs. 7 and 8 the proton and neutron occupation numbers for the ^{48}Ca nucleus. In the figures, the IPM results are indicated by the dashed lines. The black bars show the values obtained by using scalar correlations only, the gray bars those obtained with the complete operator dependent correlations.

The correlated occupation numbers are smaller than one for orbits below the Fermi surface, and larger than zero for those orbits above the Fermi surface. This effect is enhanced by the operator dependent correlations. We observe that for the states above the Fermi surface the gray bars are larger than the black ones, indicating that also for these states the operator dependent correlations, produces larger effects than the scalar ones.

We show in Fig. 9 some natural orbits for three neutron states in ^{48}Ca . In this figure, we compare the IPM results (full lines) with those obtained with scalar correlation only (dotted lines), and with the full operator dependent correlation (dashed lines). The effect of the correlations is a lowering of the peak and a small widening of the function. Despite the small effect, it is interesting to point out that this is the only case where we found that the inclusion of operator dependent terms diminishes the effect of the scalar correlation. This fact is coherent with the results on the density distributions shown in Ref. [29].

IV. QUASI-HOLE WAVE FUNCTIONS AND THE SPECTROSCOPIC FACTORS

The quasi-hole wave function is defined as:

$$\psi^t_{nljm}(x) = \sqrt{A}\frac{< \Psi_{nljm}(A-1)|\delta(x-x_A)P^t_A|\Psi(A) >}{[< \Psi_{nljm}(A-1)|\Psi_{nljm}(A-1) >< \Psi(A)|\Psi(A) >]^{1/2}} \ , \tag{25}$$

where $|\Psi_{nljm}(1,...,A-1) >$ and $|\Psi(1,...,A) >$ are the states of the nuclei formed by $A-1$ and A nucleons respectively, and P^t_A is the isospin projector. In analogy to the ansatz (3), we assume that the state of the nucleus with $A-1$ nucleons can be described as:

$$\Psi_{nljm}(A-1) = \mathcal{F}(1,...,A-1)\Phi_{nljm}(1,...,A-1) \ , \tag{26}$$

where $\Phi_{nljm}(1,...,A-1)$ is the Slater determinant obtained by removing from $\Phi(1,...,A)$ a particle characterized by the quantum numbers $nljm$, and the correlation function $\mathcal{F}$

is formed, as indicated in Eq. (5), by the two-body correlation functions f_p obtained by minimizing the A nucleon system. In an uncorrelated system the quasi-hole wave functions coincide with the hole mean-field wave functions (11).

We are interested in the radial part of the quasi-hole wave function. We obtain this quantity first by multiplying equation (25) by the vector spherical harmonics $\mathbf{Y}^{*m}_{lj}(\Omega)$, then, by integrating over the angular coordinate Ω, and, finally, by summing over m. It is useful to rewrite the radial part of the quasi-hole wave function as [33]:

$$\psi^t_{nlj}(r) = \frac{1}{2j+1}\sum_m \int d\Omega\, \mathbf{Y}^m_{lj}(\Omega)\, \psi^t_{nljm}(x) = \frac{1}{2j+1}\sum_m \mathcal{X}^t_{nljm}(r)[\mathcal{N}^t_{nlj}]^{1/2}\ , \tag{27}$$

where we have defined:

$$\mathcal{X}^t_{nljm}(r) = \sqrt{A}\frac{< \Psi^t_{nljm}(A-1)|\mathbf{Y}^{*m}_{lj}(\Omega)\,\delta(\mathbf{r}-\mathbf{r}_A)P^t_A|\Psi^t(A)>}{<\Psi^t_{nljm}(A-1)|\Psi^t_{nljm}(A-1)>}\ , \tag{28}$$

and

$$\mathcal{N}^t_{nljm} =< \frac{\Psi^t_{nljm}(A-1)|\Psi^t_{nljm}(A-1)>}{<\Psi^t(A)|\Psi^t(A)>}\ . \tag{29}$$

Following the procedure outlined in Ref. [33], we consider separately the cluster expansions of the two terms $\mathcal{N}^t_\alpha$ and $\mathcal{X}^t_\alpha$, where we have indicated with α the set of the $nljm$ quantum numbers. We obtain for $\mathcal{X}^t_\alpha$ the expression:

$$\begin{aligned}\mathcal{X}^t_\alpha(r) \;=\; & C^{t,\alpha}_{\omega,SOC}(\mathbf{r})\Bigg(R^t_{nlj}(r) + \int d^3r_1 R^t_{nlj}(r_1)P_l(\cos\theta) \\ & \times\Bigg\{g^{tt,\alpha}_{\omega d}(\mathbf{r},\mathbf{r}_1)C^{t,\alpha}_{d,pq}(\mathbf{r}_1)\Big[-\rho^{t,\alpha}_o(\mathbf{r},\mathbf{r}_1)+N^{t,\alpha}_{\omega_c c}(\mathbf{r},\mathbf{r}_1)\Big] \\ & +\rho^{t,\alpha}_o(\mathbf{r},\mathbf{r}_1) - N^{t,\alpha}_{\omega_c\rho}(\mathbf{r},\mathbf{r}_1) - N^{t,\alpha}_{\rho\rho}(\mathbf{r},\mathbf{r}_1) + \mathcal{X}^t_{SOC}(\mathbf{r},\mathbf{r}_1)\Bigg\}\Bigg)\ ,\end{aligned} \tag{30}$$

and for $\mathcal{N}^t_\alpha$ the expression:

$$\begin{aligned}\Big[\mathcal{N}^t_\alpha\Big]^{-1} \;=\; & \int d^3r C^{t,\alpha}_{d,pq}(\mathbf{r})\Bigg(|\phi^t_\alpha(\mathbf{r})|^2 + \int d^3r_1 \phi^{t*}_\alpha(\mathbf{r})\phi^t_\alpha(\mathbf{r}_1) \\ & \times 2\Big\{g^{tt,\alpha}_{dd}(\mathbf{r},\mathbf{r}_1)C^{t,\alpha}_{d,pq}(\mathbf{r}_1)\Big[-\rho^{t,\alpha}_o(\mathbf{r},\mathbf{r}_1)+N^{t,\alpha}_{cc}(\mathbf{r},\mathbf{r}_1)\Big] \\ & +\rho^{t,\alpha}_o(\mathbf{r},\mathbf{r}_1) - N^{t,\alpha}_{x\rho}(\mathbf{r},\mathbf{r}_1) - N^{t,\alpha}_{\rho\rho}(\mathbf{r},\mathbf{r}_1) + \mathcal{N}^t_{SOC}(\mathbf{r},\mathbf{r}_1)\Big\}\Bigg)\ ,\end{aligned} \tag{31}$$

The expressions of the functions $\mathcal{N}^t_{SOC}(\mathbf{r},\mathbf{r}_1)$, $\mathcal{X}^t_{SOC}(\mathbf{r},\mathbf{r}_1)$, are:

$$\mathcal{X}^{t_1}_{SOC}(\mathbf{r},\mathbf{r}_1) \;=\; \sum_{k=1}^{3} A^k \sum_{t_2=p,n}\Big[(1-\delta_{k,1})\mathcal{X}^{t_1t_2}_{2k-1,2k-1}(\mathbf{r},\mathbf{r}_1)$$

$$+\chi_1^{t_1t_2}\Big(\mathcal{X}^{t_1t_2}_{2k-1,2k}(\mathbf{r},\mathbf{r}_1)+\mathcal{X}^{t_1t_2}_{2k,2k-1}(\mathbf{r},\mathbf{r}_1)\Big)+\chi_2^{t_1t_2}\mathcal{X}^{t_1t_2}_{2k,2k}(\mathbf{r},\mathbf{r}_1)\Big]\ , \tag{32}$$

$$\mathcal{N}^{t_1}_{SOC}(\mathbf{r},\mathbf{r}_1) = \sum_{k=1}^{3}A^k\sum_{t_2=p,n}\Big[(1-\delta_{k,1})\mathcal{N}^{t_1t_2}_{2k-1,2k-1}(\mathbf{r},\mathbf{r}_1)$$
$$+\chi_1^{t_1t_2}\Big(\mathcal{N}^{t_1t_2}_{2k-1,2k}(\mathbf{r},\mathbf{r}_1)+\mathcal{X}^{t_1t_2}_{2k,2k-1}(\mathbf{r},\mathbf{r}_1)\Big)+\chi_2^{t_1t_2}\mathcal{N}^{t_1t_2}_{2k,2k}(\mathbf{r},\mathbf{r}_1)\Big]\ . \tag{33}$$

where the indexes t refer to the isospin, and we have defined:

$$\mathcal{X}^{t_1t_2}_{pq}(\mathbf{r},\mathbf{r}_1) = \frac{1}{2}\Big[h^{t_1t_2,\alpha}_{\omega,p}(\mathbf{r},\mathbf{r}_1)g^{t_1t_2,\alpha}_{\omega d}(\mathbf{r},\mathbf{r}_1)C^{t_2,\alpha}_d(\mathbf{r}_1)\Big(-\rho^{t_2,\alpha}_o(\mathbf{r},\mathbf{r}_1)+N^{t_2,\alpha}_{\omega_c c}(\mathbf{r},\mathbf{r}_1)\Big)$$
$$+g^{t_1t_2,\alpha}_{\omega d}(\mathbf{r},\mathbf{r}_1)C^{t_2,\alpha}_d(\mathbf{r}_1)N^{t_2,\alpha}_{\omega_c c,p}(\mathbf{r},\mathbf{r}_1)-N^{t_2,\alpha}_{\omega_c\rho,p}(\mathbf{r},\mathbf{r}_1)-N^{t_2,\alpha}_{\rho\rho,p}(\mathbf{r},\mathbf{r}_1)\Big]\Delta^{k_2}\ , \tag{34}$$

$$\mathcal{N}^{t_1t_2}_{pq}(\mathbf{r},\mathbf{r}_1) = \Big[h^{t_1t_2,\alpha}_{d,p}(\mathbf{r},\mathbf{r}_1)g^{t_1t_2,\alpha}_{dd}(\mathbf{r},\mathbf{r}_1)C^{t_2,\alpha}_d(\mathbf{r}_1)\Big(-\rho^{t_2,\alpha}_o(\mathbf{r},\mathbf{r}_1)+N^{t_2,\alpha}_{cc}(\mathbf{r},\mathbf{r}_1)\Big)$$
$$+g^{t_1t_2,\alpha}_{dd}(\mathbf{r},\mathbf{r}_1)C^{t_2,\alpha}_d(\mathbf{r}_1)N^{t_2,\alpha}_{cc,p}(\mathbf{r},\mathbf{r}_1)-N^{t_2,\alpha}_{x\rho,p}(\mathbf{r},\mathbf{r}_1)-N^{t_2,\alpha}_{\rho\rho,p}(\mathbf{r},\mathbf{r}_1)\Big]\Delta^{k_2}\ , \tag{35}$$

where $k_2 = 1, 2, 3$ for $q = 1, 3, 5$. The expressions of the other terms are given in Appendix A. All the quantities used in the above expressions depend on the set of quantum numbers α characterizing the quasi-hole state, since we have written the various equations by using [36]:

$$\rho^{t,\alpha}_o(\mathbf{r},\mathbf{r}_1) = \rho^t_o(\mathbf{r},\mathbf{r}_1) - \phi^{t*}_\alpha(\mathbf{r})\phi^t_\alpha(\mathbf{r}_1)\ . \tag{36}$$

The knowledge of the quasi-hole functions allows us to calculate the spectroscopic factors:

$$S^t_{nlj} = \int dr\, r_1^2\, |\psi^t_{nlj}(r)|^2\ . \tag{37}$$

The proton and neutron spectroscopic factors for the ^{12}C , ^{16}O , ^{40}Ca , ^{48}Ca and ^{208}Pb nuclei are given in Tabs. I and II for each single hole state. In these tables we compare the results obtained by using scalar correlations (f_1), with those obtained with the four central channels (f_4) and with the full correlation (f_6). The inclusion of the correlations produce spectroscopic factors smaller than one, the mean-field value. The f_6 results are smaller than those of f_4, which are smaller than those obtained with f_1.

We found that the effect of the correlations becomes larger the more bound is the state. This fact emerges by observing that for a fixed set of lj quantum numbers the spectroscopic factors increase with n, and, at the same time, that the values of the spectroscopic factors become larger when n and the lj values increase. This effect is well represented in Fig. 10 where we show with the black points the proton spectroscopic factors of the ^{208}Pb nucleus as a function of the separation energies, defined as the difference between the energy of the

A-nucleons system and that of the correspondent $A-1$-nucleons system. We have associated the spectroscopic factor of each level to its empirical separation energy.

In Fig. 10 our results are compared with the empirical spectroscopic factors [12], extracted from (e,e'p) experiments, and represented by the white diamonds. The good agreement indicates the importance of the correlations in understanding the empirical values of the spectroscopic factors. However, for the more external shells, the data are smaller than our results. We surmise that this difference is related to correlations, of long-range type, which are not well described by our theory.

As example of correlation effects, we show in Fig. 11 the squares of the proton $3s_{1/2}$ and neutron $3p_{1/2}$ quasi-hole wave functions. The correlations lower the wave function in the nuclear interior. Also in this case, the effect of the correlations increases together with the number of operator channels considered.

In Fig. 12 we show with a gray band the difference between the empirical charge distributions of ^{206}Pb and ^{205}Tl [19]. The dashed dotted line, labeled as IPM, has been obtained by considering that the difference between the two charge distributions can be described as a single $3s_{1/2}$ proton hole in the core of the lead nucleus. This curve has been obtained by folding the IPM line of Fig. 11 with the electric proton form factor in its dipole form. In a slightly more elaborated picture, the ground state of the ^{205}Tl is composed by the $3s_{1/2}$ proton hole in the ^{206}Pb ground state, plus the coupling of the $2d_{5/2}$ and $2d_{3/2}$ proton levels with the first 2^+ excited state of ^{206}Pb [37, 38]. This description of the ^{205}Tl charge distribution, shown by the dotted line in the figure, is still within the IPM framework. The dashed line has been obtained by adding to the dotted line the core polarization effects produced by long-range correlations. These effects have been calculated by following the Random Phase Approximation approach of Refs. [39, 40]. The full line has been obtained when our SRC effects are also included.

The various effects presented in Fig. 12 have been obtained in different theoretical frameworks, and the final result does not have any pretense of being a well grounded and coherent description of the empirical charge differences. The point we want to make by showing this figure is that the effects of the SRC are of the same order of magnitude of those commonly considered in traditional nuclear structure calculations.

V. SUMMARY AND CONCLUSIONS

In this work we have extended the FHNC/SOC scheme in order to calculate the OBDM's, the natural orbits and the quasi-hole wave functions of finite nuclear systems non saturated in isospin, and in jj coupling representation of the single particle wave function basis. Our results have been obtained by using the two-body realistic interaction Argonne v_8' and the associated three-body interaction Urbana IX. The calculations have been done by using operator dependent correlations which include terms up to the tensor ones.

We found that the correlations enhance by orders of magnitude the high-energy tail of the nucleon momentum distribution. The occupation numbers of the natural orbits below the Fermi level, are depleted, and the opposite happens for those above the Fermi level. Also the values of the spectroscopic factors are depleted with respect to the IPM, and our results are in good agreement with the empirical values. We have shown that the results of models considering expansions up to the first order correlation lines, provide only qualitative descriptions of the SRC effects. In the description of the charge density difference between ^{206}Pb and ^{205}Tl, the SRC effects are of comparable size of those commonly considered in traditional nuclear structure calculations based on effective theories.

A general outcome of our study, is that the effects of the correlations increase with the complexity of the correlation function. This means that operator dependent correlations enhance the effects produced by the scalar correlations. This not obvious result, is valid in general, not always. We have shown in Ref. [29], that scalar and operator dependent correlations have destructive interference effects on the density distributions. We found in the present study an analogous behavior regarding the natural orbits. These quantities are related to the density distributions. It seems that the effects of the SRC are rather straightforward on quantities which involve two-nucleons, while they are more difficult to predict on quantities related to single nucleon dynamics. On these last quantities, however, these SRC effects are very small, usually negligible.

In this work, we have highlighted a set of effects that cannot be described by mean field based effective theories. The description of the nucleus in kinematics regimes where these effects are relevant, requires the use of microscopic theories.

VI. ACKNOWLEDGMENTS

This work has been partially supported by the agreement INFN-CICYT, by the Spanish Ministerio de Educación y Ciencia (FIS2005-02145) and by the MURST through the PRIN: *Teoria della struttura dei nuclei e della materia nucleare*.

APPENDIX A

For sake of completeness, we give in this appendix the detailed expression of the OBDM for finite nuclear systems not saturated in isospin, and in jj coupling scheme of the single particle wave function basis (11). The notation for the nodal functions N and for the vertex corrections C is that used in Ref. [33]. The indexes t_1, t_2, t_3 indicate protons and neutrons, and the subscript j is related to the antiparallel spin states.

For the correlated OBDM we obtain the expression:

$$\begin{aligned}\rho^t(\mathbf{r}_1,\mathbf{r}_{1'}) \;=\; & 2C^t_{\omega,SOC}(\mathbf{r}_1)C^t_{\omega,SOC}(\mathbf{r}_{1'})e^{N^t_{\omega\omega}(\mathbf{r}_1,\mathbf{r}_{1'})}\Big[\rho^t_o(\mathbf{r}_1,\mathbf{r}_{1'}) - N^t_{\omega_c\omega_c}(\mathbf{r}_1,\mathbf{r}_{1'})\Big] + \\ & 2C^t_{\omega}(\mathbf{r}_1)C^t_{\omega}(\mathbf{r}_{1'})e^{N^t_{\omega\omega}(\mathbf{r}_1,\mathbf{r}_{1'})} \\ & \times\sum_{p>1} A^k\Delta^k\Big\{N^t_{\omega\omega,p}(\mathbf{r}_1,\mathbf{r}_{1'})\Big[\rho^t_o(\mathbf{r}_1,\mathbf{r}_{1'}) - N^t_{\omega_c\omega_c}(\mathbf{r}_1,\mathbf{r}_{1'})\Big] - N^t_{\omega_c\omega_c,p}(\mathbf{r}_1,\mathbf{r}_{1'})\Big\}\ .\end{aligned} \tag{A1}$$

In the above equation, k has been defined as in Eq. (20), and we have used $\Delta^{k=1,2,3} = 1-\delta_{k,3}$, and $A^{k=1,2,3} = 1,3,6$.

In the following we shall calculate the expectation value of the isospin operator sequence:

$$\chi^{t_1t_2}_n = \chi^*_{t_1}(1)\chi^*_{t_2}(2)\left(\boldsymbol{\tau}_1\cdot\boldsymbol{\tau}_2\right)^n\chi_{t_1}(1)\chi_{t_2}(2)\ ,$$

by considering that

$$\left(\boldsymbol{\tau}_i\cdot\boldsymbol{\tau}_j\right)^n = a_n + (1-a_n)\boldsymbol{\tau}_i\cdot\boldsymbol{\tau}_j\ ,$$

with

$$a_{n+1} = 3(1-a_n) \qquad \text{and} \qquad a_0 = 1\ .$$

By using the above equations we have that:

$$\chi^{t_1t_2}_0 = 1 \quad , \quad \chi^{t_1t_2}_1 = 2\delta_{t_1t_2} - 1 \quad \text{and} \quad \chi^{t_1t_2}_n = 2a_n - 1 + 2(1-a_n)\delta_{t_1t_2}\ .$$

The expressions of the vertex corrections are:

$$C^{t_1}_{\omega,SOC}(\mathbf{r}_1) = C^{t_1}_{\omega}(\mathbf{r}_1)\Big[1 + U^{t_1}_{\omega,SOC}(\mathbf{r}_1)\Big]\ , \tag{A2}$$

$$U^{t_1}_{\omega,SOC}(\mathbf{r}_1) = \sum_{k=1}^{3} A^k \sum_{t_2=p,n} \Big[(1-\delta_{k,1}) U^{t_1t_2}_{\omega,2k-1,2k-1}(\mathbf{r}_1) + \chi_1^{t_1t_2}\Big(U^{t_1t_2}_{\omega,2k-1,2k}(\mathbf{r}_1) + U^{t_1t_2}_{\omega,2k,2k-1}(\mathbf{r}_1)\Big) + \chi_2^{t_1t_2} U^{t_1t_2}_{\omega,2k,2k}(\mathbf{r}_1)\Big] , \quad \text{(A3)}$$

where we have defined

$$U^{t_1t_2}_{\omega,pq}(\mathbf{r}_1) = \int d\mathbf{r}_2 h^{t_1t_2}_{\omega,p}(r_{12}) \Bigg\{ \Big[g^{t_1t_2}_{\omega d}(\mathbf{r}_1,\mathbf{r}_2) C^{t_2}_{d,pq}(\mathbf{r}_2) + g^{t_1t_2}_{\omega e}(\mathbf{r}_1,\mathbf{r}_2) C^{t_2}_{e,pq}(\mathbf{r}_2)\Big] N^{t_1t_2}_{\omega d,q}(\mathbf{r}_1,\mathbf{r}_2) + g^{t_1t_2}_{\omega d}(\mathbf{r}_1,\mathbf{r}_2) C^{t_2}_{e,pq}(\mathbf{r}_2) N^{t_1t_2}_{\omega e,q}(\mathbf{r}_1,\mathbf{r}_2) \Bigg\} , \quad \text{(A4)}$$

$$h^{t_1t_2}_{\omega,p}(\mathbf{r}_1,\mathbf{r}_2) = \frac{f_p(r_{12})}{f_1(r_{12})} + (1-\delta_{p,1}) N^{t_1t_2}_{\omega d,p}(\mathbf{r}_1,\mathbf{r}_2) . \quad \text{(A5)}$$

The expressions of the two-body distribution functions for $p > 1$ are:

$$g^{t_1}_{\omega\omega,p}(\mathbf{r}_1,\mathbf{r}_{1'}) = g^{t_1}_{\omega\omega}(\mathbf{r}_1,\mathbf{r}_{1'}) N^{t_1}_{\omega\omega,p}(\mathbf{r}_1,\mathbf{r}_{1'}) , \quad \text{(A6)}$$

$$g^{t_1t_2}_{\omega d,p}(\mathbf{r}_1,\mathbf{r}_2) = h^{t_1t_2}_{\omega,p}(\mathbf{r}_1,\mathbf{r}_2) g^{t_1t_2}_{\omega d}(\mathbf{r}_1,\mathbf{r}_2) = N^{t_1t_2}_{\omega d,p}(\mathbf{r}_1,\mathbf{r}_2) + X^{t_1t_2}_{\omega d,p}(\mathbf{r}_1,\mathbf{r}_2) , \quad \text{(A7)}$$

$$g^{t_1t_2}_{\omega e,p}(\mathbf{r}_1,\mathbf{r}_2) = h^{t_1t_2}_{\omega,p}(\mathbf{r}_1,\mathbf{r}_2) g^{t_1t_2}_{\omega e}(\mathbf{r}_1,\mathbf{r}_2) + g^{t_1t_2}_{\omega d}(\mathbf{r}_1,\mathbf{r}_2) N^{t_1t_2}_{\omega e,p}(\mathbf{r}_1,\mathbf{r}_2) = X^{t_1t_2}_{\omega e,p}(\mathbf{r}_1,\mathbf{r}_2) + N^{t_1t_2}_{\omega e,p}(\mathbf{r}_1,\mathbf{r}_2) , \quad \text{(A8)}$$

$$g^{t_1}_{\omega_c c,p}(\mathbf{r}_1,\mathbf{r}_2) = h^{t_1t_1}_{\omega,p}(\mathbf{r}_1,\mathbf{r}_2) g^{t_1}_{\omega_c c}(\mathbf{r}_1,\mathbf{r}_2) + g^{t_1t_1}_{\omega d}(\mathbf{r}_1,\mathbf{r}_2) N^{t_1}_{\omega_c c,p}(\mathbf{r}_1,\mathbf{r}_2) = X^{t_1}_{\omega_c c,p}(\mathbf{r}_1,\mathbf{r}_2) + N^{t_1}_{\omega_c c,p}(\mathbf{r}_1,\mathbf{r}_2) . \quad \text{(A9)}$$

Finally the nodals functions are expressed as:

$$N^{t_1}_{mn(j),p}(1,2) = N^{t_1}_{mnx(j),p}(1,2) + N^{t_1}_{m\rho(j),p}(1,2) + N^{t_1}_{\rho n(j),p}(1,2) + N^{t_1}_{\rho,p}(1,2) , \quad \text{(A10)}$$

with $m, n = c, w_c$. The separation of the above nodal diagrams in four terms, corresponds to the classification in the xx, $x\rho$, ρx and $\rho\rho$ parts [29], and it has been applied to the quantities $N^{t_1t_3}_{mn(j),pqr}(1,2)$ defined in the following.

$$N^{t_1}_{mm,2k_1-1}(1,1') = \sum_{k_2k_3=1}^{3} \sum_{t_3=p,n} \Big[N^{t_1t_3}_{mm,2k_1-1,2k_2-1,2k_3-1}(1,1') + \chi_1^{t_1t_3}[N^{t_1t_3}_{mm,2k_1-1,2k_2,2k_3-1}(1,1') + N^{t_1t_3}_{mm,2k_1-1,2k_2-1,2k_3}(1,1')]\Big] , \quad \text{(A11)}$$

$$N^{t_1t_2}_{mm,2k_1}(1,1') = \sum_{k_2,k_3=1}^{3} \sum_{t_3=p,n} \chi_2^{t_1t_3} N^{t_1t_3}_{mm,2k_1,2k_2,2k_3}(1,1') , \quad \text{(A12)}$$

$$N^{t_1t_2}_{\omega n,2k_1-1}(1,2) = \sum_{k_2k_3=1}^{3} \sum_{t_3=p,n} \Big[N^{t_1t_2t_3}_{\omega n,2k_1-1,2k_2-1,2k_3-1}(1,2) \quad \text{(A13)}$$

$$+\ \chi_1^{t_1t_3}N^{t_1t_2t_3}_{\omega n,2k_1-1,2k_2,2k_3-1}(1,2)+\chi_1^{t_2t_3}N^{t_1t_2t_3}_{\omega n,2k_1-1,2k_2-1,2k_3}(1,2)\Big]\ ,$$

$$N^{t_1t_2}_{\omega n,2k_1}(1,2)\ =\ \sum_{k_2,k_3=1}^{3}\sum_{t_3=p,n}N^{t_1t_2t_3}_{\omega n,2k_1,2k_2,2k_3}(1,2)\ , \tag{A14}$$

$$N^{t_1}_{\omega_c c(j),2k_1-1}(1,2)\ =\ \sum_{k_2,k_3=1}^{3}\sum_{t_3=p,n}\Big[N^{t_1t_3}_{\omega_c c(j),2k_1-1,2k_2-1,2k_3-1}(1,2) \tag{A15}$$

$$+\ \chi_1^{t_1t_3}[N^{t_1t_3}_{\omega_c c(j),2k_1-1,2k_2,2k_3-1}(1,2)+N^{t_1t_3}_{\omega_c c(j),2k_1-1,2k_2-1,2k_3}(1,2)]\Big]$$

$$N^{t_1}_{\omega_c c(j),2k_1}(1,2)\ =\ \sum_{k_2,k_3=1}^{3}\sum_{t_3=p,n}N^{t_1t_3}_{\omega_c c(j),2k_1,2k_2,2k_3}(1,2)\ . \tag{A16}$$

with $m=w,w_c$ and $n=d,e$.

$$N^{t_1t_3}_{\omega\omega,pqr}(\mathbf{r}_1,\mathbf{r}_{1'})\ =\ \Big[X^{t_1t_3}_{\omega d,q}(\mathbf{r}_1,\mathbf{r}_2)\xi^{k_2k_3k_1}_{121'}C^{t_3}_{d,qr}(\mathbf{r}_2)|X^{t_3t_1}_{d\omega,r}(\mathbf{r}_2,\mathbf{r}_{1'})+N^{t_3t_1}_{d\omega,r}(\mathbf{r}_2,\mathbf{r}_{1'})\Big]+ \tag{A17}$$

$$\Big[X^{t_1t_3}_{\omega e,q}(\mathbf{r}_1,\mathbf{r}_2)\xi^{k_2k_3k_1}_{121'}C^{t_3}_{e,qr}(\mathbf{r}_2)|X^{t_3t_1}_{d\omega,r}(\mathbf{r}_2,\mathbf{r}_{1'})+N^{t_3t_1}_{d\omega,r}(\mathbf{r}_2,\mathbf{r}_{1'})\Big]+$$

$$\Big[X^{t_1t_3}_{\omega d,q}(\mathbf{r}_1,\mathbf{r}_2)\xi^{k_2k_3k_1}_{121'}C^{t_3}_{e,qr}(\mathbf{r}_2)|X^{t_3t_1}_{e\omega,sr}(\mathbf{r}_2,\mathbf{r}_{1'})+N^{t_3t_1}_{e\omega,r}(\mathbf{r}_2,\mathbf{r}_{1'})\Big]\ ,$$

$$N^{t_1t_2t_3}_{\omega n,pqr}(\mathbf{r}_1,\mathbf{r}_2)\ =\ \Big[X^{t_1t_3}_{\omega d,q}(\mathbf{r}_1,\mathbf{r}_3)\xi^{k_2k_3k_1}_{132}C^{t_3}_{d,qr}(\mathbf{r}_3)|X^{t_3t_2}_{dn,r}(\mathbf{r}_3,\mathbf{r}_2)+N^{t_3t_2}_{dn,r}(\mathbf{r}_3,\mathbf{r}_2)\Big]+ \tag{A18}$$

$$\Big[X^{t_1t_3}_{\omega e,q}(\mathbf{r}_1,\mathbf{r}_3)\xi^{k_2k_3k_1}_{132}C^{t_3}_{e,qr}(\mathbf{r}_3)|X^{t_3t_2}_{dn,r}(\mathbf{r}_3,\mathbf{r}_2)+N^{t_3t_2}_{dn,r}(\mathbf{r}_3,\mathbf{r}_2)\Big]+$$

$$\Big[X^{t_1t_3}_{\omega d,q}(\mathbf{r}_1,\mathbf{r}_3)\xi^{k_2k_3k_1}_{132}C^{t_3}_{e,qr}(\mathbf{r}_3)|X^{t_3t_2}_{en,r}(\mathbf{r}_3,\mathbf{r}_2)+N^{t_3t_2}_{en,r}(\mathbf{r}_3,\mathbf{r}_2)\Big] \tag{A19}$$

also in the above equations we used $n=d,e$. In the following equations we have that $m,n=c,w_c$.

$$N^{t_1t_3}_{mnx,pqr}(1,2)\ =\ \Big[X^{t_1}_{mc,q}(1,3)\xi^{k_2k_3k_1}_{132}\frac{\Delta^{k_3}}{2}C^{t_3}_{e,qr}(3)|X^{t_3}_{cn}(3,2)+N^{t_3}_{cnx}(3,2)+N^{t_3}_{\rho n}(3,2)\Big]+$$

$$(1-\delta_{r,1})\times \tag{A20}$$

$$\Big[X^{t_1}_{mc}(1,3)\xi^{k_2k_3k_1}_{132}\frac{\Delta^{k_2}}{2}C^{t_3}_{e,qr}(3)|X^{t_3}_{cn,r}(3,2)+N^{t_3}_{cnx,r}(3,2)+N^{t_3}_{\rho n,r}(3,2)\Big]-$$

$$\delta_{k_11}\delta_{k_21}\delta_{k_31}\Big\{\Big[X^{t_1}_{mcj,q}(1,3)\frac{1}{2}C^{t_3}_{e,qr}(3)|X^{t_3}_{cnj}(3,2)+N^{t_3}_{cnxj}(3,2)+N^{t_3}_{\rho nj}(3,2)\Big]$$

$$+(1-\delta_{r,1})\Big[X^{t_1}_{mcj}(1,3)\frac{1}{2}C^{t_3}_{e,qr}(3)|X^{t_3}_{cnj,r}(3,2)+N^{t_3}_{cnxj,r}(3,2)+N^{t_3}_{\rho nj,r}(3,2)\Big]\Big\}\ ,$$

$$N^{t_1t_3}_{m\rho,pqr}(1,2)\ =\ \Big[X^{t_1}_{mc,q}(1,3)\xi^{k_2k_3k_1}_{132}\frac{\Delta^{k_3}}{2}C^{t_3}_{e,qr}(3)|-\rho^{t_3}_{o}(3,2)+N^{t_3}_{c\rho}(3,2)+N^{t_3}_{\rho}(3,2)\Big]$$

$$+(1-\delta_{r,1})\Big[X^{t_1}_{mc}(1,3)\xi^{k_2k_3k_1}_{132}\frac{\Delta^{k_2}}{2}C^{t_3}_{e,qr}(3)|N^{t_3}_{c\rho,r}(3,2)+N^{t_3}_{\rho,r}(3,2)\Big]-$$

$$\delta_{k_11}\delta_{k_21}\delta_{k_31}\Big\{\Big[X^{t_1}_{mcj,q}(1,3)\frac{1}{2}C^{t_3}_{e,qr}(3)|-\rho^{t_3}_{oj}(3,2)+N^{t_3}_{c\rho j}(3,2)+N^{t_3}_{\rho j}(3,2)\Big]$$

$$+(1-\delta_{r,1})\Big[X^{t_1}_{mcj}(1,3)\frac{1}{2}C^{t_3}_{e,qr}(3)|N^{t_3}_{c\rho j,r}(3,2)+N^{t_3}_{\rho j,r}(3,2)\Big]\Big\}\ , \tag{A21}$$

$$N^{t_1t_3}_{\rho,pqr}(1,2) = -\Big[\rho^{t_1}_0(1,3)\xi^{k_2k_3k_1}_{132}\frac{\Delta^{k_2}}{2}C^{t_3}_{e,qr}(3)|N^{t_3}_{c\rho,r}(3,2)\Big] \tag{A22}$$
$$-\Big[\rho^{t_1}_0(1,3)\xi^{k_2k_3k_1}_{132}\frac{\Delta^{k_2}}{2}(C^{t_3}_{e,qr}(3)-1)|N^{t_3}_{\rho,r}(3,2)-\delta_{r,1}\rho^{t_3}_0(3,2)\Big]$$
$$+\delta_{k_11}\delta_{k_21}\delta_{k_31}\Big\{\Big[\rho^{t_1}_{0j}(1,3)\frac{1}{2}C^{t_3}_{e,qr}(3)|N^{t_3}_{c\rho j,r}(3,2)\Big]$$
$$+\Big[\rho^{t_1}_{0j}(1,3)\frac{1}{2}(C^{t_3}_{e,qr}(3)-1)|N^{t_3}_{\rho j,r}(3,2)-\delta_{r,1}\rho^{t_3}_{0j}(3,2)\Big]\Big\}\ ,$$

$$N^{t_1t_3}_{mnxj,pqr}(1,2) = \delta_{k_11}\delta_{k_21}\delta_{k_31}\Big\{\Big[X^{t_1}_{mc,q}(1,3)\frac{1}{2}C^{t_3}_{e,qr}(3)|X^{t_3}_{cnj}(3,2)+N^{t_3}_{cnxj}(3,2)+N^{t_3}_{\rho nj}(3,2)\Big]+$$
$$(1-\delta_{r,1})\Big[X^{t_1}_{mc}(1,3)\frac{1}{2}C^{t_3}_{e,qr}(3)|X^{t_3}_{cnj,r}(3,2)+N^{t_3}_{cnxj,r}(3,2)+N^{t_3}_{\rho nj,r}(3,2)\Big]+$$
$$\Big[X^{t_1}_{mcj,q}(1,3)\frac{1}{2}C^{t_3}_{e,qr}(3)|X^{t_3}_{cn}(3,2)+N^{t_3}_{cnx}(3,2)+N^{t_3}_{\rho n}(3,2)\Big]+$$
$$(1-\delta_{r,1})\Big[X^{t_1}_{mcj}(1,3)\frac{1}{2}C^{t_3}_{e,qr}(3)|X^{t_3}_{cn,r}(3,2)+N^{t_3}_{cnx,r}(3,2)+N^{t_3}_{\rho n,r}(3,2)\Big]\Big\}\ , \tag{A23}$$

$$N^{t_1t_3}_{m\rho j,pqr}(1,2) = \delta_{k_11}\delta_{k_21}\delta_{k_31}\Big\{\Big[X^{t_1}_{mc,q}(1,3)\frac{1}{2}C^{t_3}_{e,qr}(3)|-\rho^{t_3}_{oj}(3,2)+N^{t_3}_{c\rho j}(3,2)+N^{t_3}_{\rho j}(3,2)\Big]$$
$$+(1-\delta_{r,1})\Big[X^{t_1}_{mc}(1,3)\frac{1}{2}C^{t_3}_{e,qr}(3)|N^{t_3}_{c\rho j,r}(3,2)+N^{t_3}_{\rho j,r}(3,2)\Big]$$
$$+\Big[X^{t_1}_{mcj,q}(1,3)\frac{1}{2}C^{t_3}_{e,qr}(3)|-\rho^{t_3}_{o}(3,2)+N^{t_3}_{c\rho}(3,2)+N^{t_3}_{\rho}(3,2)\Big]+$$
$$(1-\delta_{r,1})\Big[X^{t_1}_{mcj}(1,3)\frac{1}{2}C^{t_3}_{e,qr}(3)|N^{t_3}_{c\rho,r}(3,2)+N^{t_3}_{\rho,r}(3,2)\Big]\Big\}\ , \tag{A24}$$

$$N^{t_1t_3}_{\rho j,pqr}(1,2) = -\delta_{k_11}\delta_{k_21}\delta_{k_31}\Big\{\Big[\rho^{t_1}_0(1,3)\frac{1}{2}C^{t_3}_{e,qr}(3)|N^{t_3}_{c\rho j,r}(3,2)\Big]$$
$$+\Big[\rho^{t_1}_0(1,3)\frac{1}{2}(C^{t_3}_{e,qr}(3)-1)|N^{t_3}_{\rho j,r}(3,2)-\delta_{r,1}\rho^{t_3}_{0j}(3,2)\Big]$$
$$+\Big[\rho^{t_1}_{0j}(1,3)\frac{1}{2}C^{t_3}_{e,qr}(3)|N^{t_3}_{c\rho,r}(3,2)\Big]$$
$$+\Big[\rho^{t_1}_{0j}(1,3)\frac{1}{2}(C^{t_3}_{e,qr}(3)-1)|N^{t_3}_{\rho,r}(3,2)-\delta_{r,1}\rho^{t_3}_0(3,2)\Big]\Big\}\ . \tag{A25}$$

The values of the ξ^{k_1,k_2,k_3}_{ijk} coefficients are given in Ref. [41].

---

[1] H. Kamada et al., Phys. Rev. C **64**, 044001 (2001).

[2] B. S. Pudliner, V. R. Pandharipande, J. Carlson, S. Pieper, and R. B. Wiringa, Phys. Rev. C **56**, 1720 (1997).

[3] S. C. Pieper, Nucl. Phys. A **751**, 516 (2005).

[4] K. A. Brueckner, Phys. Rev. **97**, 1353 (1955).

[5] K. Nakayama, S. Krewald, and J. Speth, Nucl. Phys. A **451**, 243 (1985).

[6] S. K. Bogner, T. T. S. Kuo, and A. Schwenk, Phys. Rep. **386**, 1 (2003).

[7] L. Coraggio, A. Covello, A. Gargano, N. Itaco, and T. T. S. Kuo, Phys. Rev. C **73**, 014304 (2006).

[8] R. Roth, T. Neff, H. Hergert, and H. Feldmeier, Nucl. Phys. A **745**, 3 (2004).

[9] R. Roth, P. Papakonstantinou, N. Paar, H. Hergert, T. Neff, and H. Feldmeier, Phys. Rev. C **73**, 044312 (2006).

[10] L. Lapikas, Nucl. Phys. A **553**, 297c (1993).

[11] G. J. Kramer, H. P. Blok, and L. Lapikas, Nucl. Phys. A **679**, 267 (2001).

[12] M. F. van Batenburg, Ph.D. thesis, Universiteit Utrecht (Nederlands) (2001), unpublished.

[13] E. M. N. Quint, Ph.D. thesis, Universiteit Amsterdam (Nederlands) (1988), unpublished.

[14] S. Boffi, C. Giusti, and F. D. Pacati, Phys. Rep. A **226**, 1 (1993).

[15] J. Lichtenstadt et al., Phys. Rev. C **20**, 497 (1979).

[16] C. E. Hyde-Wright et al., Phys. Rev. C **35**, 880 (1987).

[17] C. J. G. Onderwater et al., Phys. Rev. Lett. **78**, 4893 (1997).

[18] C. J. G. Onderwater et al., Phys. Rev. Lett. **81**, 2213 (1998).

[19] J. M. Cavedon et al., Phys. Rev. Lett. **49**, 978 (1982).

[20] C. Papanicolas, *Nuclear structure at high spin, excitation and momentum transfer,* H. Nann ed. (American Institute of Physics, New York, 1986).

[21] W. H. Dickhoff and C. Barbieri, Prog. Part. Nucl. Phys. **52**, 377 (2004).

[22] P. Navrátil, J. P. Vary, and B. R. Barrett, Phys. Rev. C **62**, 054311 (2000).

[23] C. Forssén, P. Navrátil, W. E. Ormand, and E. Caurier, Phys. Rev. C **71**, 044312 (2005).

[24] J. H. Heisenberg and B. Mihaila, Phys. Rev. C **59**, 1440 (1999).

[25] B. Mihaila and J. H. Heisenberg, Phys. Rev. C **60**, 054303 (1999).

[26] G. Co', A. Fabrocini, S. Fantoni, and I. E. Lagaris, Nucl. Phys. A **549**, 439 (1992).

[27] R. B. Wiringa, V. Ficks, and A. Fabrocini, Phys. Rev. C **38**, 1010 (1988).

[28] A. Akmal, V. Pandharipande, and D. G. Ravenhall, Phys. Rev. C **58**, 1804 (1998).

[29] C. Bisconti, F. Arias de Saavedra, G. Co', and A. Fabrocini, Phys. Rev. C **73**, 054304 (2006).

[30] A. R. Edmonds, *Angular momentum in quantum mechanics* (Princeton University Press, Princeton, 1957).

[31] G. Co', A. Fabrocini, and S. Fantoni, Nucl. Phys. A **568**, 73 (1994).

[32] F. Arias de Saavedra, G. Co', A. Fabrocini, and S. Fantoni, Nucl. Phys. A **605**, 359 (1996).

[33] A. Fabrocini and G. Co', Phys. Rev. C **63**, 044319 (2001).

[34] A. N. Antonov, P. E. Hodgson, and I. Z. Petkov, *Nucleon momentum and density distributions* (Clarendon, Oxford, 1988).

[35] F. Arias de Saavedra, G. Co', and M. M. Renis, Phys. Rev. C **55**, 673 (1997).

[36] F. Arias de Saavedra, G. Co', and A. Fabrocini Phys. Rev. C **63**, 064308 (2001).

[37] V. K. L. Zamick and J. Speth, Nucl. Phys. **245**, 365 (1975).

[38] V. Klemt and J. Speth, Z. Phys. A **278**, 59 (1976).

[39] G. Co' and J. Speth, Z. Phys. A **326**, 361 (1987).

[40] M. Anguiano and G. Co', Jour. Phys. G **27**, 2109 (2001).

[41] V. R. Pandharipande and R. B. Wiringa, Rev. Mod. Phys. **51**, 821 (1979).

nlj	^{12}C			^{16}O			^{40}Ca			^{48}Ca			^{208}Pb		
	f_1	f_4	f_6	f_1	f_4	f_6	f_1	f_4	f_6	f_1	f_4	f_6	f_1	f_4	f_6
$1s_{1/2}$	0.96	0.95	0.91	0.95	0.90	0.85	0.93	0.84	0.78	0.94	0.85	0.78	0.93	0.83	0.77
$1p_{3/2}$	0.96	0.96	0.94	0.96	0.93	0.89	0.95	0.87	0.82	0.95	0.87	0.81	0.94	0.83	0.77
$1p_{1/2}$				0.96	0.93	0.89	0.95	0.87	0.81	0.95	0.83	0.80	0.94	0.83	0.77
$1d_{5/2}$							0.96	0.90	0.86	0.96	0.90	0.85	0.94	0.84	0.79
$2s_{1/2}$							0.96	0.92	0.87	0.94	0.92	0.86	0.94	0.86	0.80
$1d_{3/2}$							0.95	0.90	0.85	0.96	0.90	0.84	0.94	0.84	0.79
$1f_{7/2}$													0.94	0.86	0.81
$2p_{3/2}$													0.95	0.87	0.82
$1f_{5/2}$													0.95	0.86	0.80
$2p_{1/2}$													0.95	0.87	0.82
$1g_{9/2}$													0.95	0.88	0.83
$1g_{7/2}$													0.94	0.88	0.82
$2d_{5/2}$													0.95	0.89	0.83
$1h_{11/2}$													0.94	0.90	0.86
$2d_{3/2}$													0.95	0.89	0.83
$3s_{1/2}$													0.95	0.90	0.85

TABLE I: Proton spectroscopic factors of the ^{12}C , ^{16}O , ^{40}Ca , ^{48}Ca and ^{208}Pb nuclei. We present the results obtained by using the scalar correlation only (f_1), the first four operator channels of the correlation (f_4) and the full correlation operator (f_6).

nlj	^{12}C			^{16}O			^{40}Ca			^{48}Ca			^{208}Pb		
	f_1	f_4	f_6	f_1	f_4	f_6	f_1	f_4	f_6	f_1	f_4	f_6	f_1	f_4	f_6
$1s_{12}$	0.96	0.95	0.91	0.95	0.90	0.85	0.93	0.84	0.78	0.93	0.86	0.80	0.92	0.85	0.80
$1p_{3/2}$	0.96	0.96	0.94	0.96	0.93	0.89	0.95	0.87	0.82	0.94	0.88	0.83	0.93	0.85	0.80
$1p_{1/2}$				0.96	0.93	0.89	0.95	0.87	0.81	0.94	0.88	0.82	0.93	0.85	0.80
$1d_{5/2}$							0.96	0.90	0.86	0.95	0.90	0.86	0.93	0.86	0.82
$2s_{1/2}$							0.96	0.92	0.87	0.95	0.92	0.87	0.93	0.88	0.84
$1d_{3/2}$							0.95	0.90	0.85	0.95	0.90	0.86	0.93	0.86	0.82
$1f_{7/2}$										0.95	0.94	0.91	0.94	0.88	0.84
$2p_{3/2}$													0.94	0.89	0.85
$1f_{5/2}$													0.93	0.88	0.84
$2p_{1/2}$													0.94	0.89	0.85
$1g_{9/2}$													0.94	0.90	0.86
$1g_{7/2}$													0.94	0.90	0.86
$2d_{5/2}$													0.94	0.91	0.87
$1h_{11/2}$													0.94	0.93	0.89
$2d_{3/2}$													0.94	0.90	0.87
$3s_{1/2}$													0.94	0.92	0.88
$2f_{7/2}$													0.95	0.93	0.90
$1h_{9/2}$													0.94	0.92	0.88
$2f_{5/2}$													0.95	0.93	0.90
$3p_{3/2}$													0.95	0.94	0.90
$1i_{13/2}$													0.94	0.93	0.90
$3p_{1/2}$													0.95	0.94	0.90

TABLE II: The same as Tab. I for neutron states.

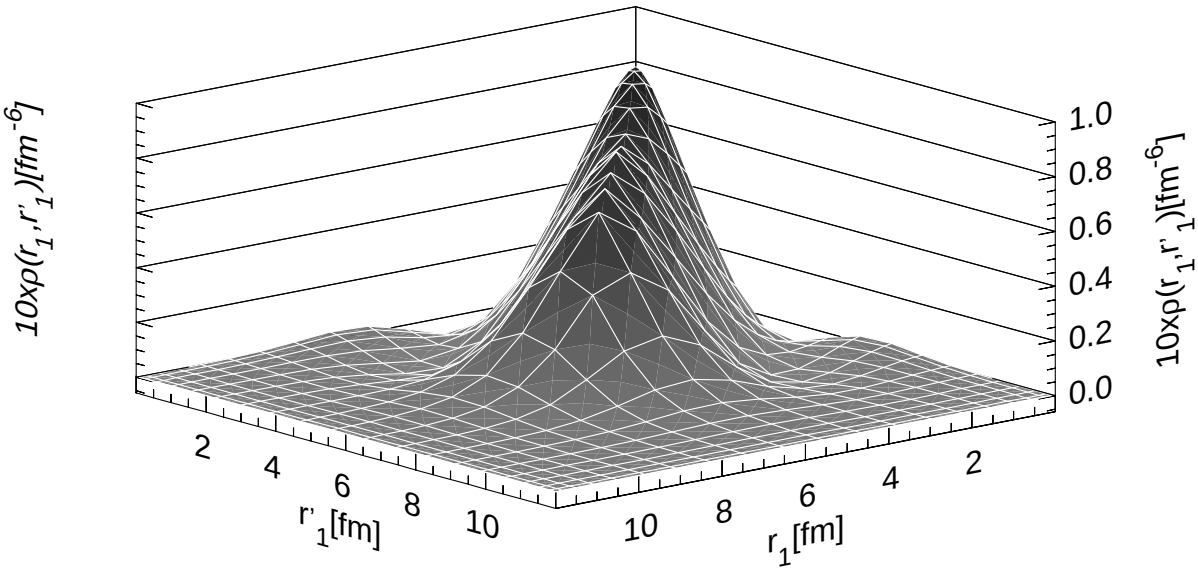

FIG. 1: The proton one-body density matrix, $\rho(r_1, r_1')$, for the ^{208}Pb nucleus in FHNC/SOC approximation, calculated for $\theta_{11'}$=0. The diagonal part $\rho(r_1, r_1)$ is the proton density distribution.

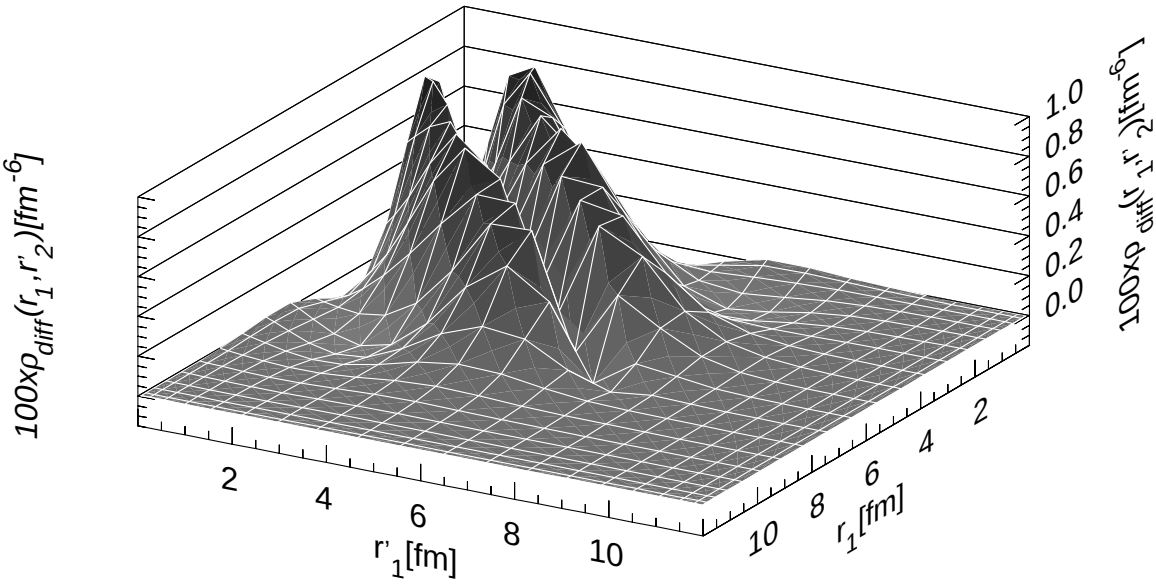

FIG. 2: The difference $\rho_o(r_1, r_1') - \rho(r_1, r_1')$, between the proton IPM one-body density matrix of the ^{208}Pb nucleus, and that obtained with our FHNC/SOC calculations. The two density matrices, have been calculated for $\theta_{11'}$=0. Note that the scale here is ten times larger than that of Fig. 1.

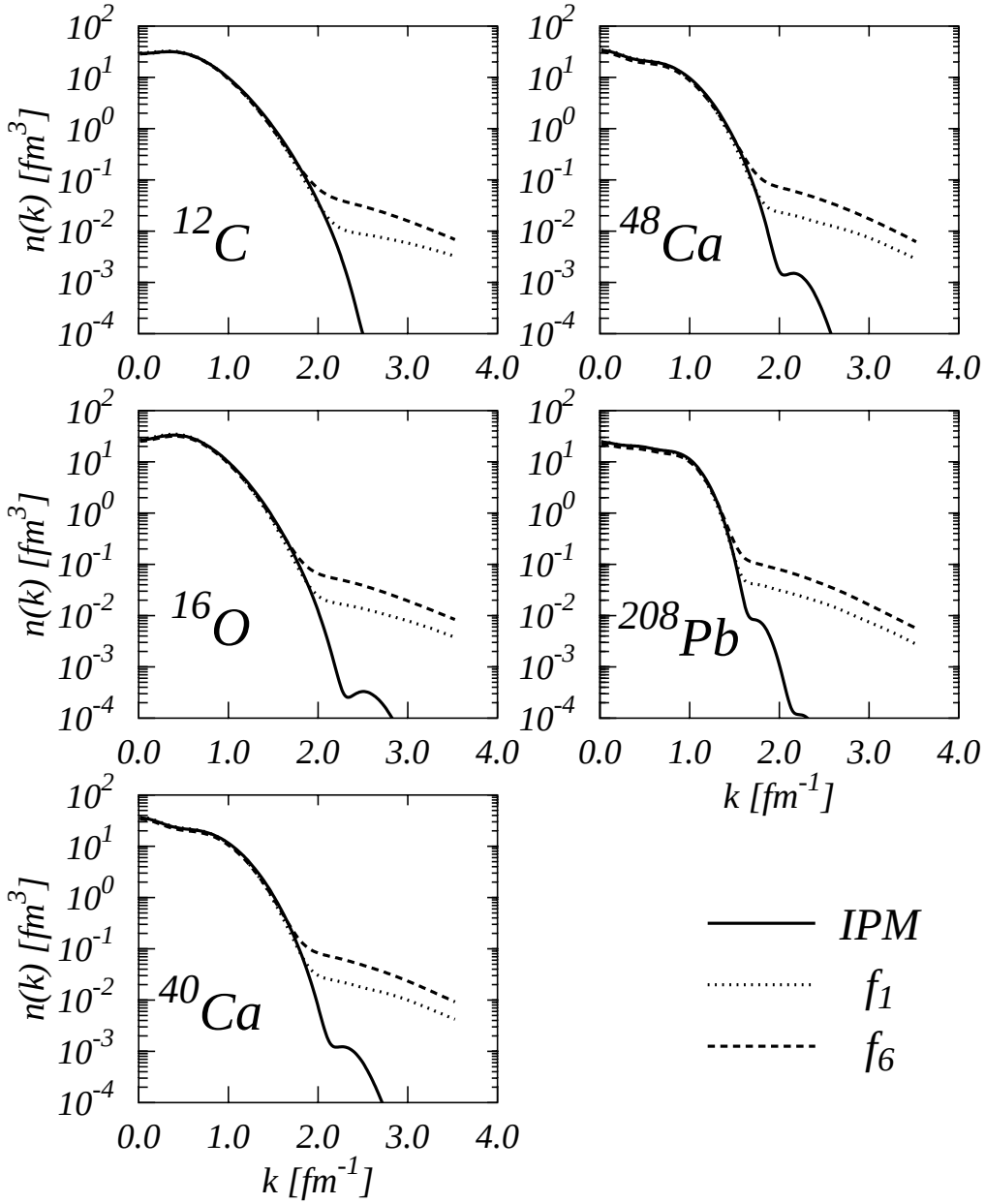

FIG. 3: The proton momentum distributions of the ^{12}C , ^{16}O , ^{40}Ca , ^{48}Ca and ^{208}Pb nuclei calculated in the IPM model, by using the scalar correlations only (f_1) and the full operator dependent correlations (f_6).

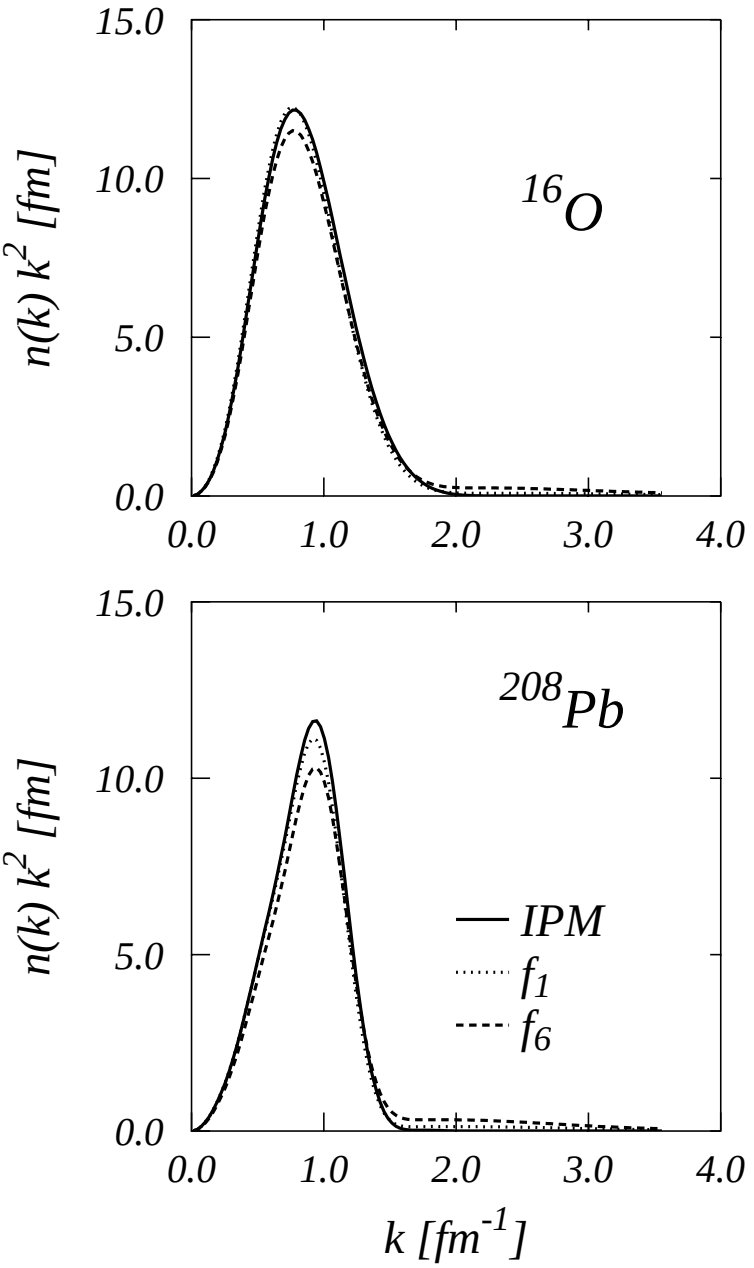

FIG. 4: The proton momentum distributions of the ^{16}O and ^{208}Pb nuclei multiplied by k^2. The full lines show the IPM results, the dotted lines have been obtained by using scalar correlations only, and the dashed lines with the complete correlation.

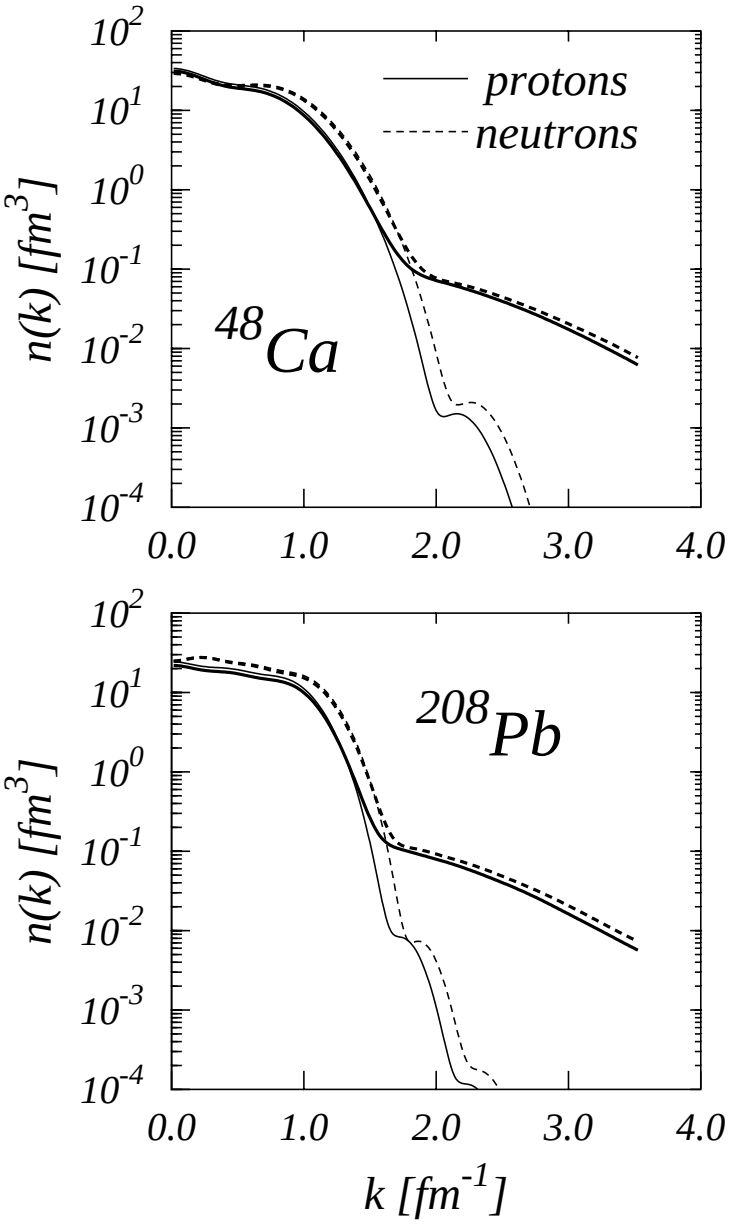

FIG. 5: Proton (full lines) and neutron (dashed lines) momentum distributions of the ^{48}Ca and ^{208}Pb . The thick lines show the results of our calculations, the thin lines the IPM results.

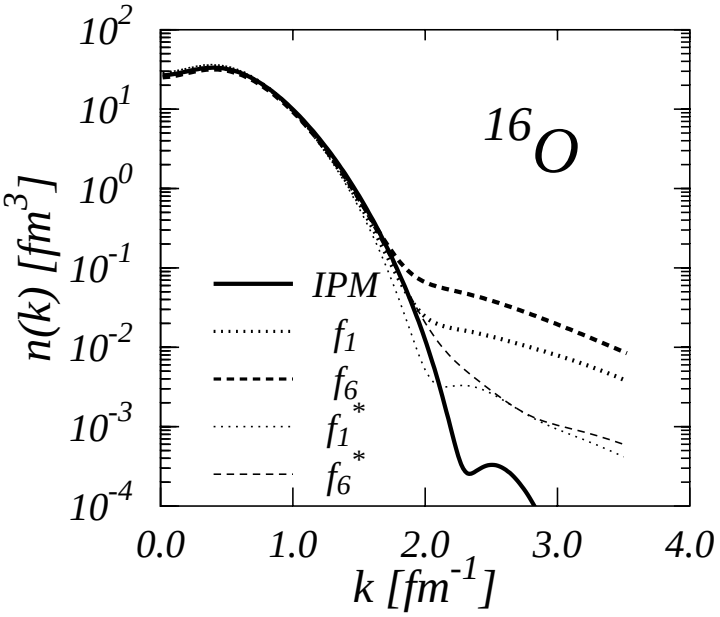

FIG. 6: Proton momentum distribution of ^{16}O in various approximations. The thick lines are those of the analogous panel of Fig. 3. The thin lines have been obtained by using the first-order expansion method of Ref. [35].

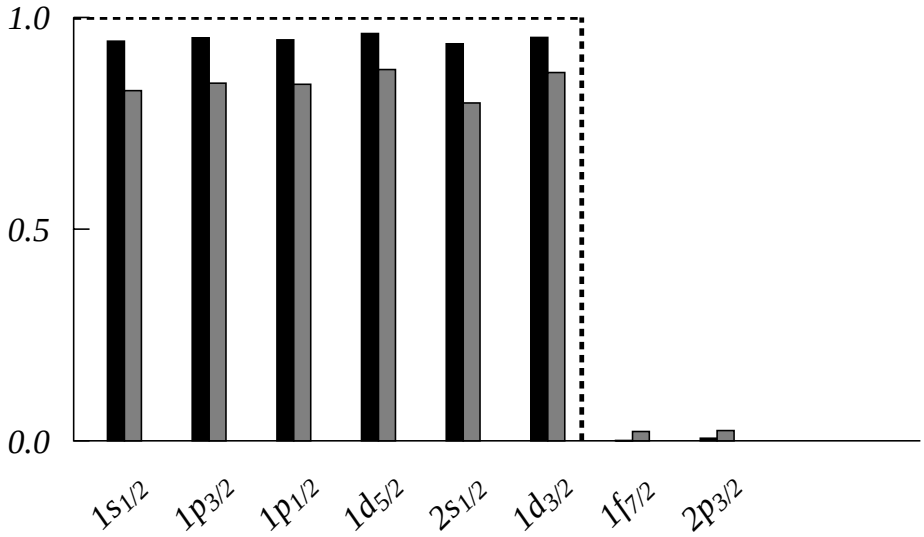

FIG. 7: Occupation numbers of the proton natural orbits of the ^{48}Ca nucleus. The dashed line indicates the IPM values. The black bars show the values obtained with the scalar corrrelation and the gray bars those values obtained with the full correlation.

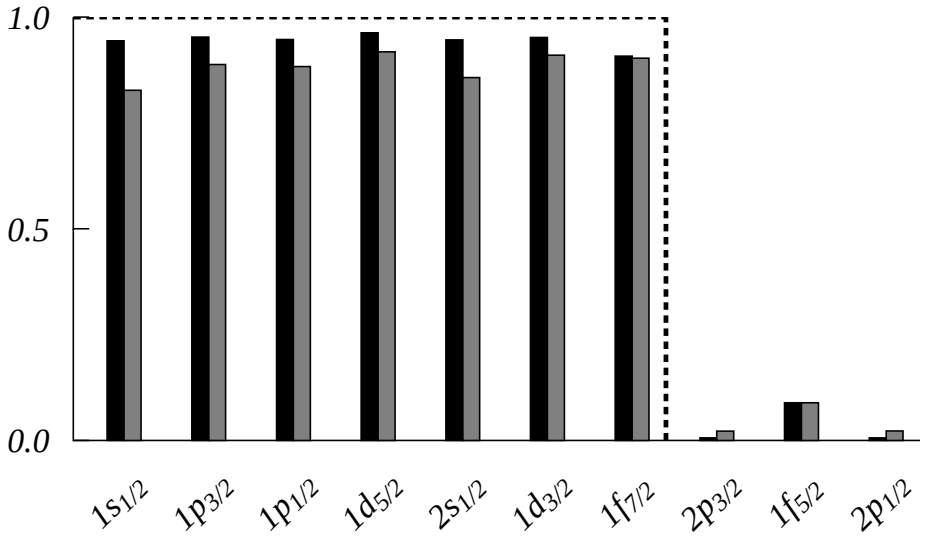

FIG. 8: The same as Fig. 7 for the occupation numbers of the neutron natural orbits of the ^{48}Ca nucleus.

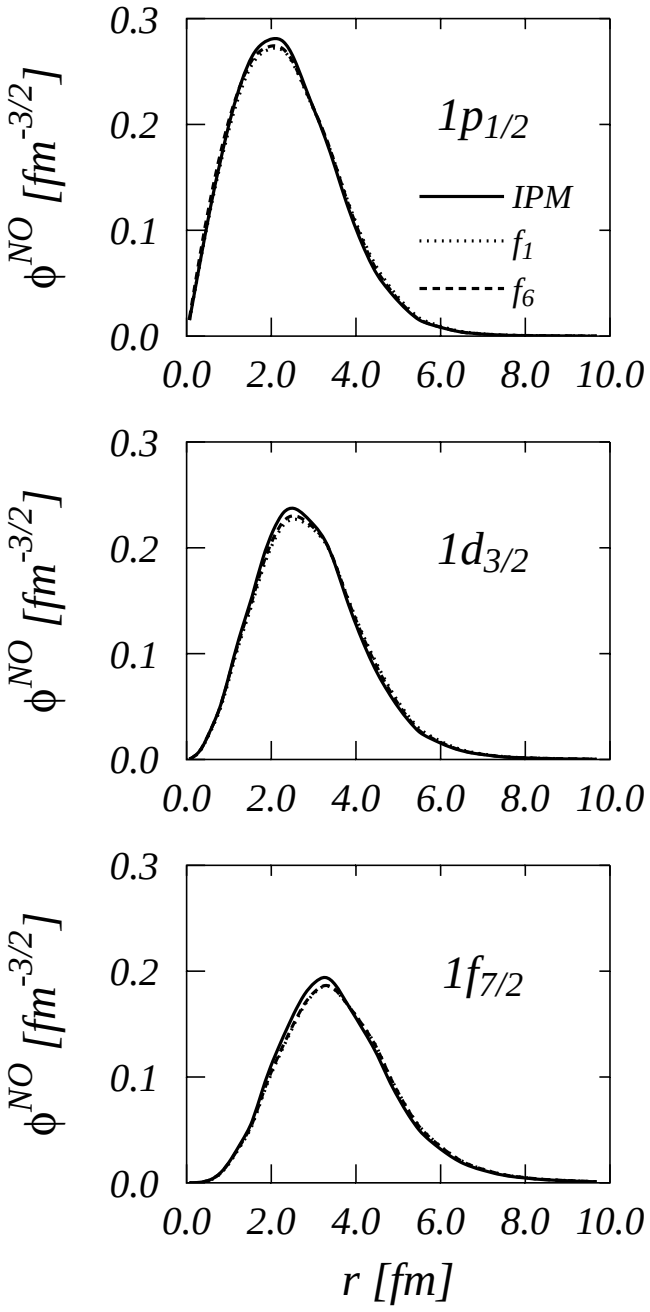

FIG. 9: Natural orbits for some neutron states in ^{48}Ca . The full lines show the IPM orbits, the dotted lines those obtained with scalar correlations only and the dashed lines those obtained with the complete operator dependent correlation.

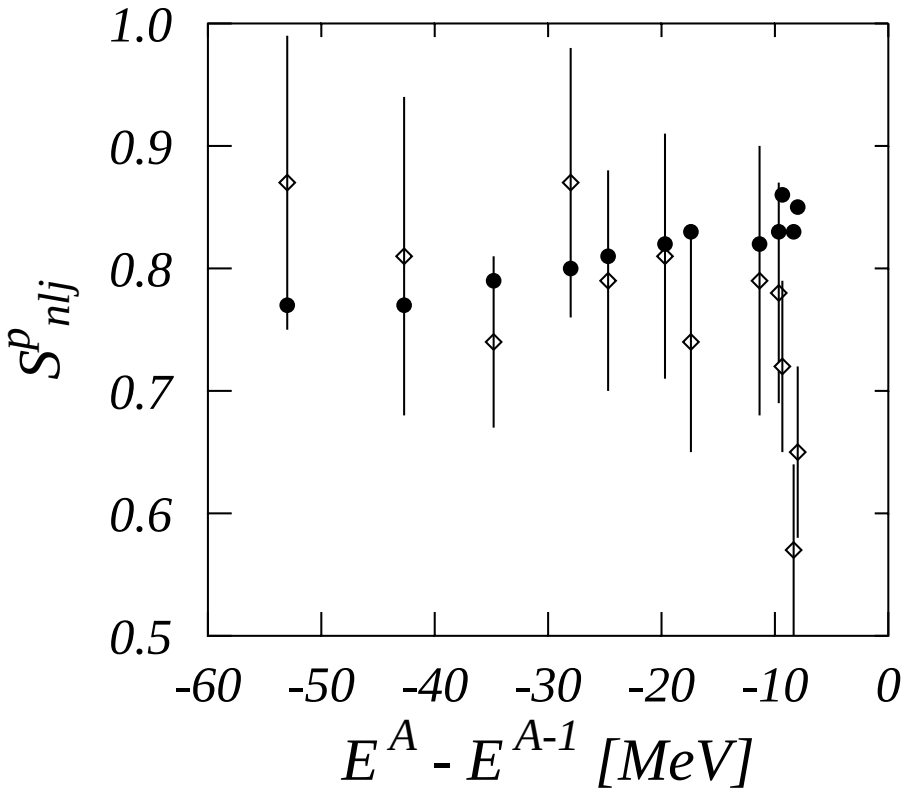

FIG. 10: Proton spectroscopic factors of the ^{208}Pb nucleus as a function of the separation energies. The black points show our results, and the white diamonds the empirical values extracted from (e,e'p) experiments [12].

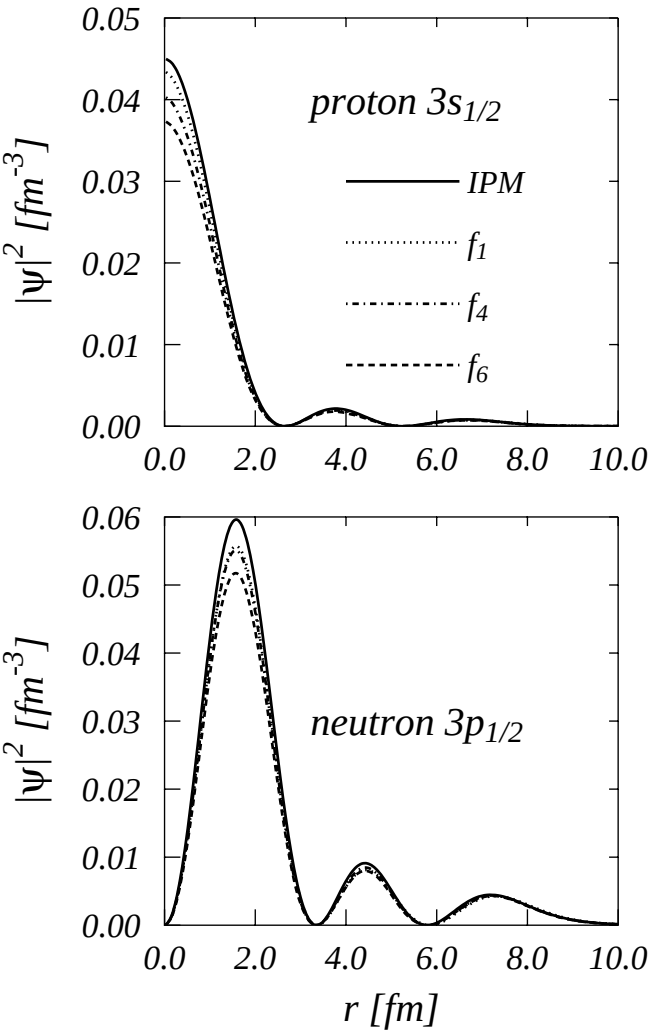

FIG. 11: Proton $3s_{1/2}$ and neutron $3p_{1/2}$ quasi-hole functions, squared, of the ^{208}Pb nucleus. The various lines show the results obtained by using different type of correlations.

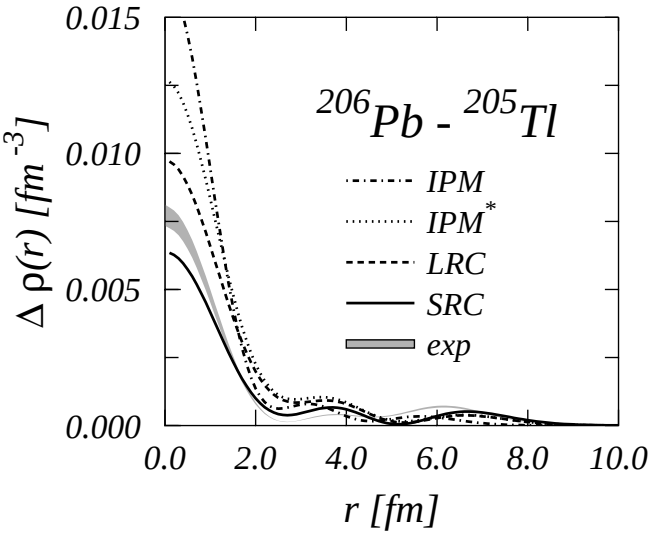

FIG. 12: Differences between charge density distributions of ^{206}Pb and ^{205}Tl. See the text for the explanation of the various lines.